**Supplementary Materials**

# Top-down synthesis of three-dimension $ABO_3$-type perovskite oxides with rich grain boundaries and lattice defects for molecular oxygen activation in catalytic oxidation reactions

**Shan Wang[1,2,#], Yu Luo[1,#], Shuai Lyu[1], Yashi Chen[1], Ping Xiao[1], Junjiang Zhu[1,*]**

[1]Hubei Key Laboratory of Biomass Fibers and Eco-dyeing & Finishing, School of Chemistry and Chemical Engineering, Wuhan Textile University, Wuhan 430200, Hubei, China.
[2]College of Pharmacy, Dali University, Dali 671000, Yunnan, China.
[#]Authors contributed equally.

[*]**Correspondence to:** Prof Junjiang Zhu, Hubei Key Laboratory of Biomass Fibers and Eco-dyeing & Finishing, School of Chemistry and Chemical Engineering, Wuhan Textile University, Wuhan 430200, Hubei, China. E-mail: jjzhu@wtu.edu.cn

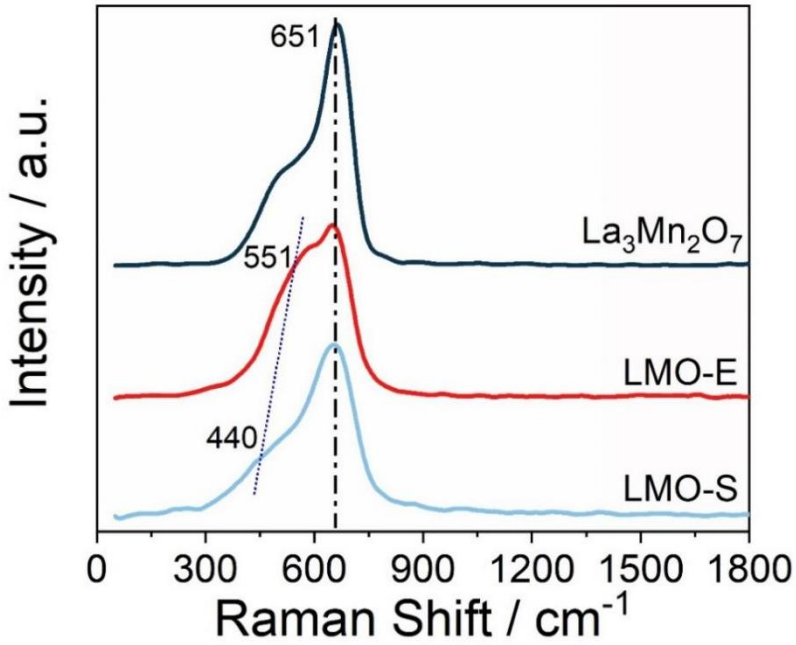


**Supplementary Figure 1.** Raman spectra of LMO-S, LMO-E and $La_3Mn_2O_7$.

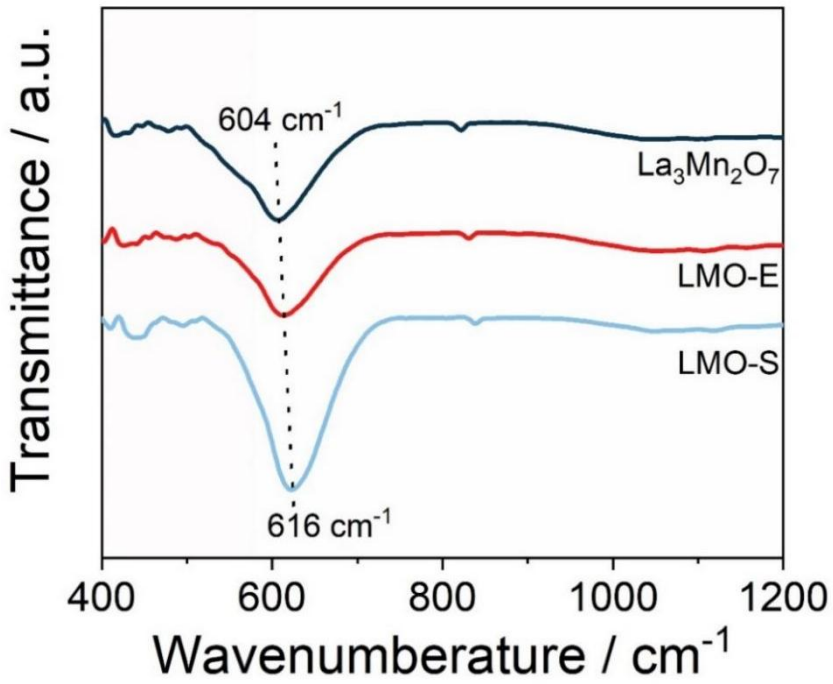


**Supplementary Figure 2.** FT-IR spectra of LMO-S, LMO-E and $La_3Mn_2O_7$.

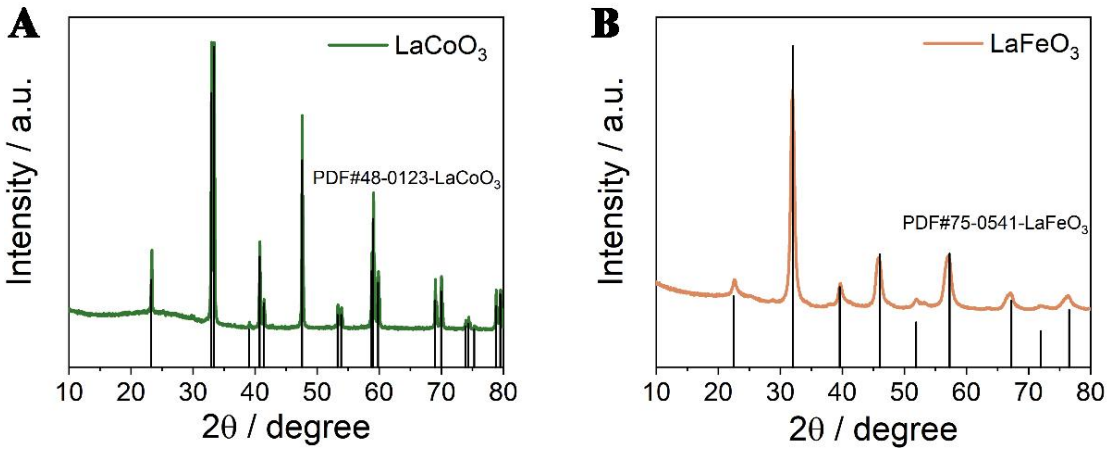


**Supplementary Figure 3.** X-ray diffraction patterns of (A) $LaCoO_3$ and (B) $LaFeO_3$ prepared by the herein proposed "top-down" method.

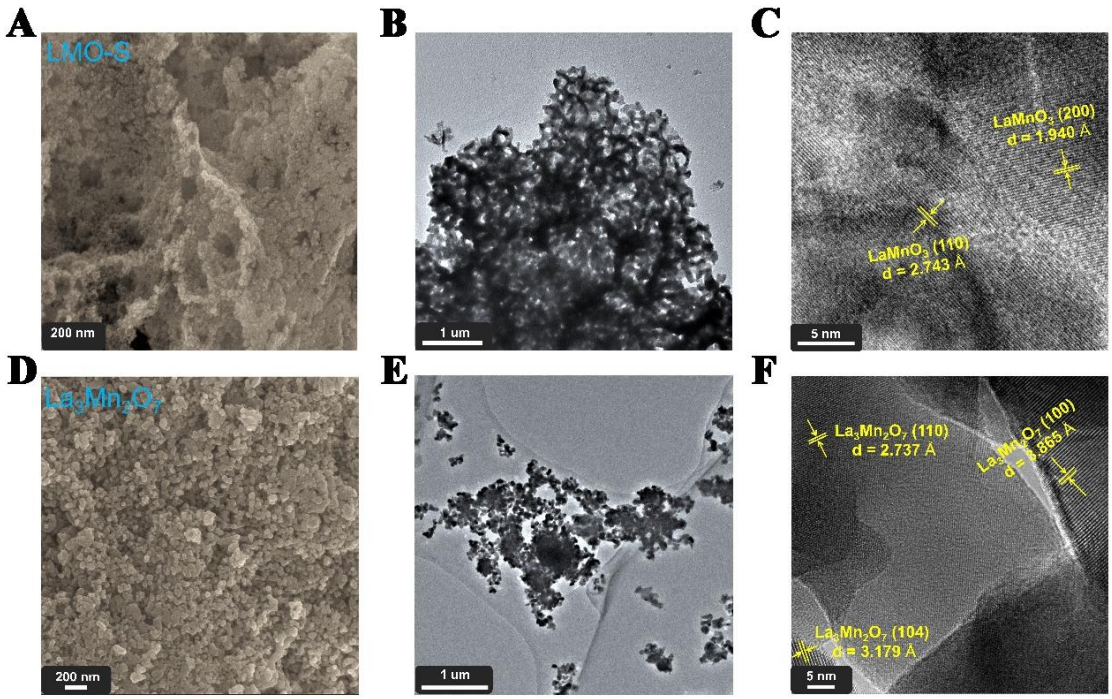


**Supplementary Figure 4.** SEM images of (A) LMO-S and (D) $La_3Mn_2O_7$; TEM images of (B and C) LMO-S and (E and F) $La_3Mn_2O_7$.

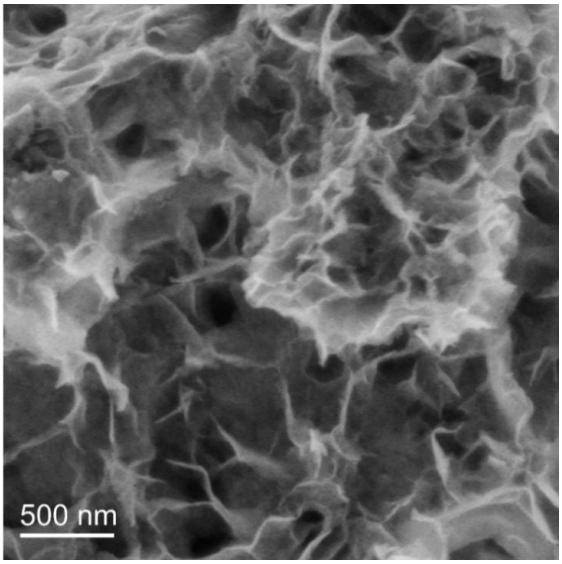


**Supplementary Figure 5.** SEM images of LMO-E.

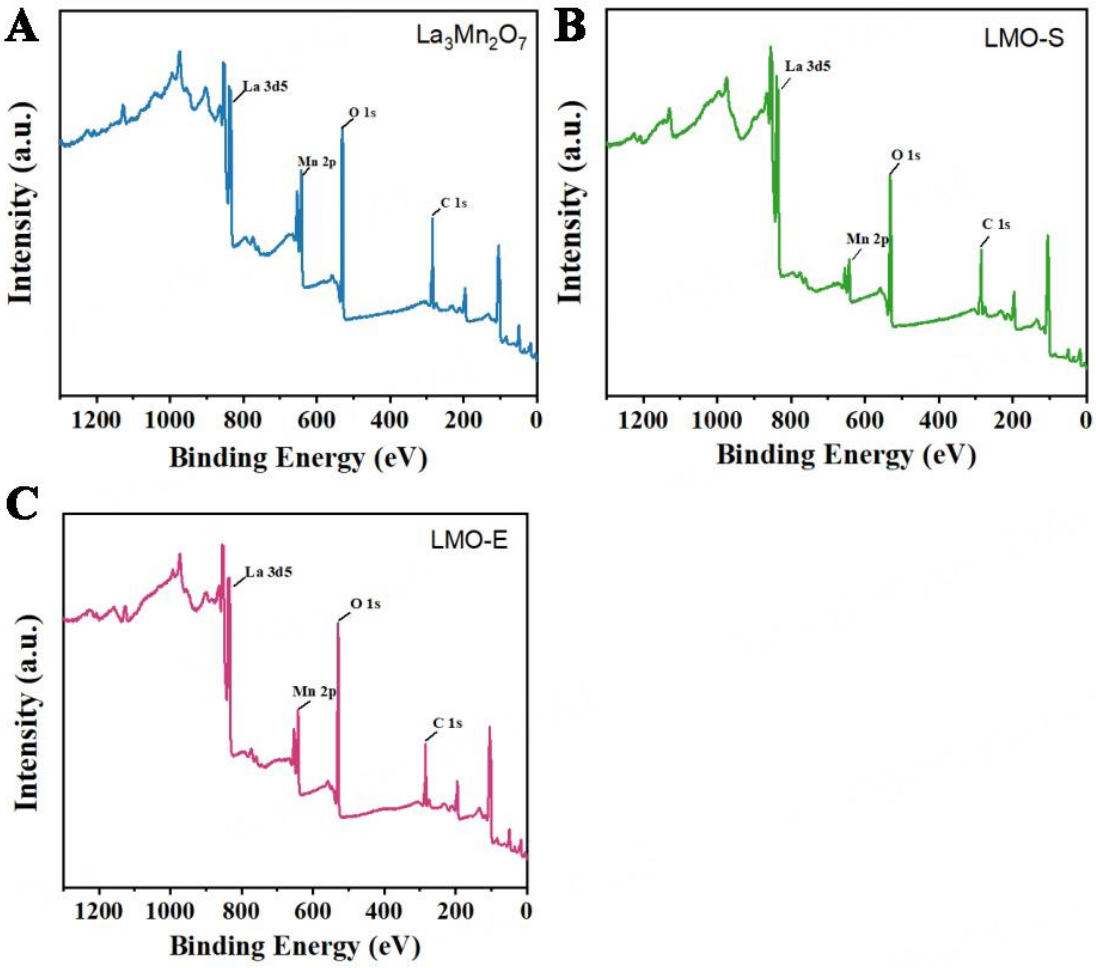


**Supplementary Figure 6.** XPS survey spectrum of (A) $La_3Mn_2O_7$, (B) LMO-S and (C) LMO-E.

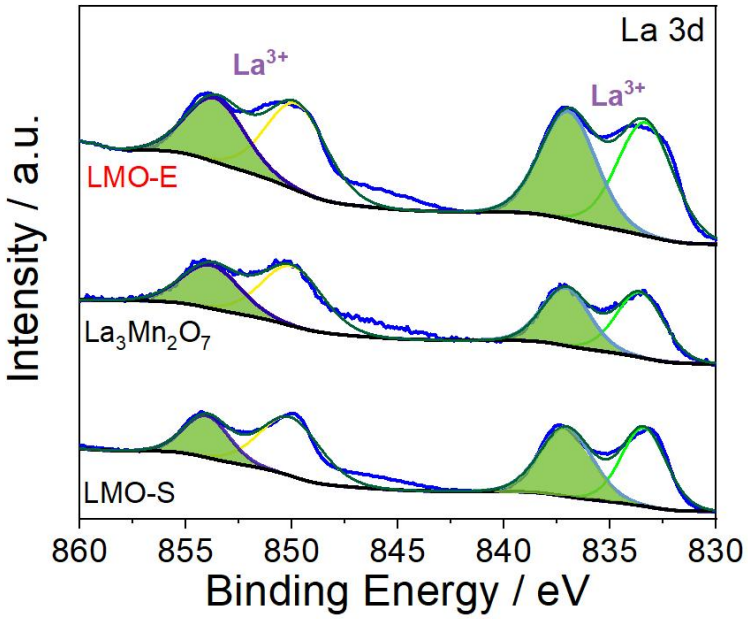


**Supplementary Figure 7.** La 3d XPS spectra of LMO-S, LMO-E and $La_3Mn_2O_7$.

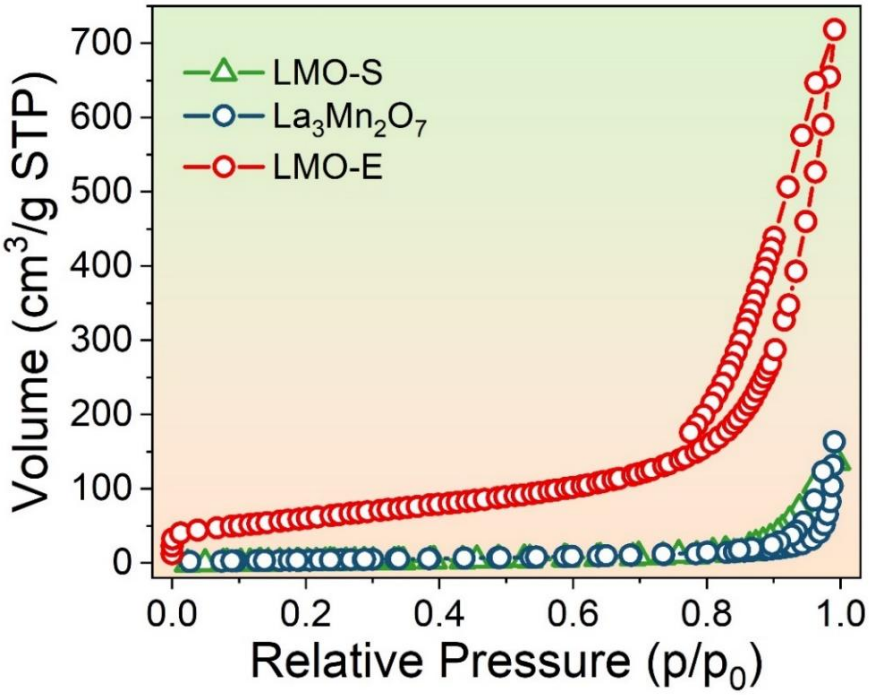


**Supplementary Figure 8.** $N_2$ physisorption isotherms of LMO-S, LMO-E and $La_3Mn_2O_7$.

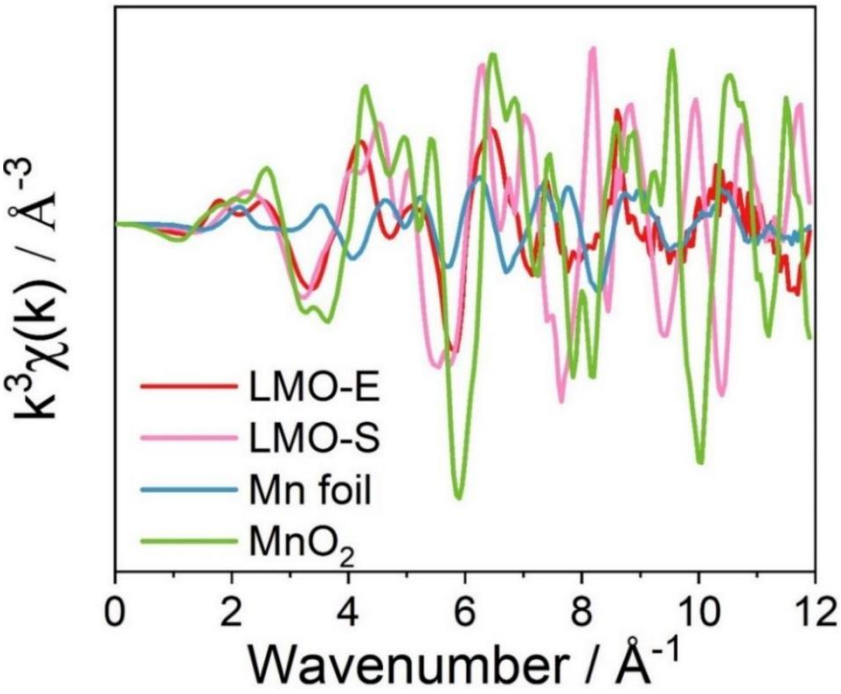


**Supplementary Figure 9.** FT-EXAFS spectra and fits of Mn K-edges of LMO-S and LMO-E samples.

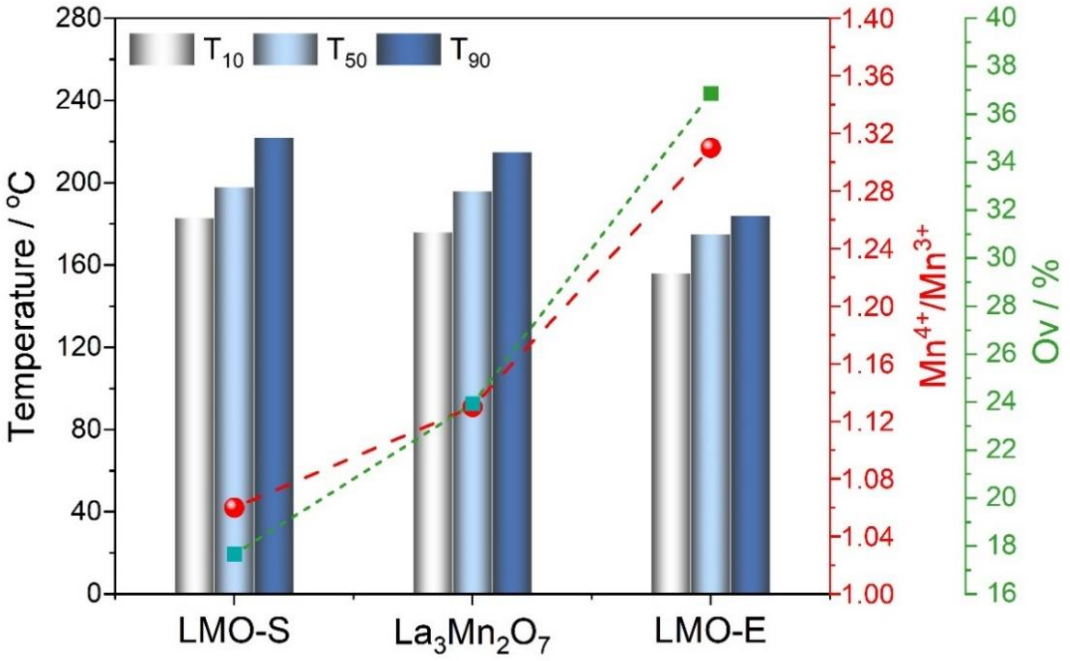


**Supplementary Figure 10.** Correlations between the catalytic activity and the ratios of the surface species recorded for the LMO-S, $La_3Mn_2O_7$ and LMO-E catalyst.

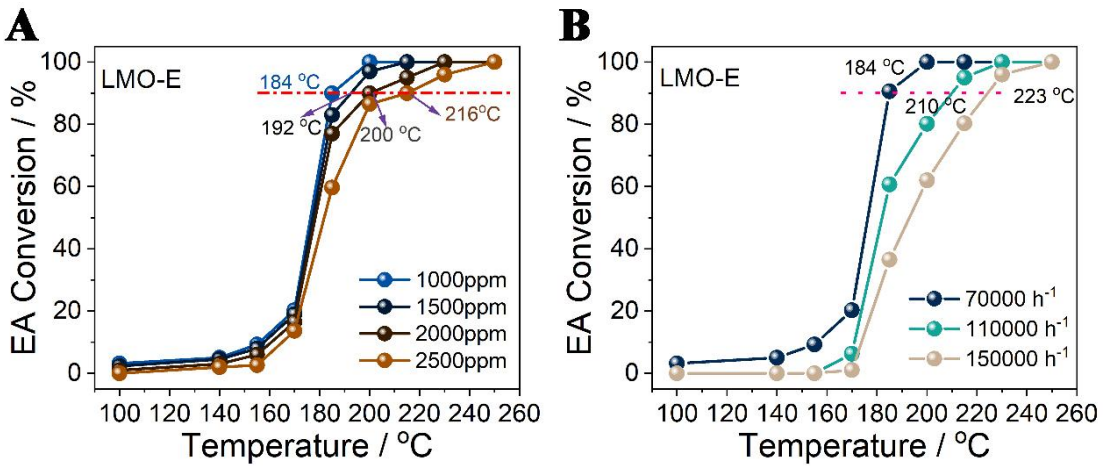


**Supplementary Figure 11.** Catalytic performances of LMO-E for EA oxidation under (A) different EA concentrations and (B) different GHSV.

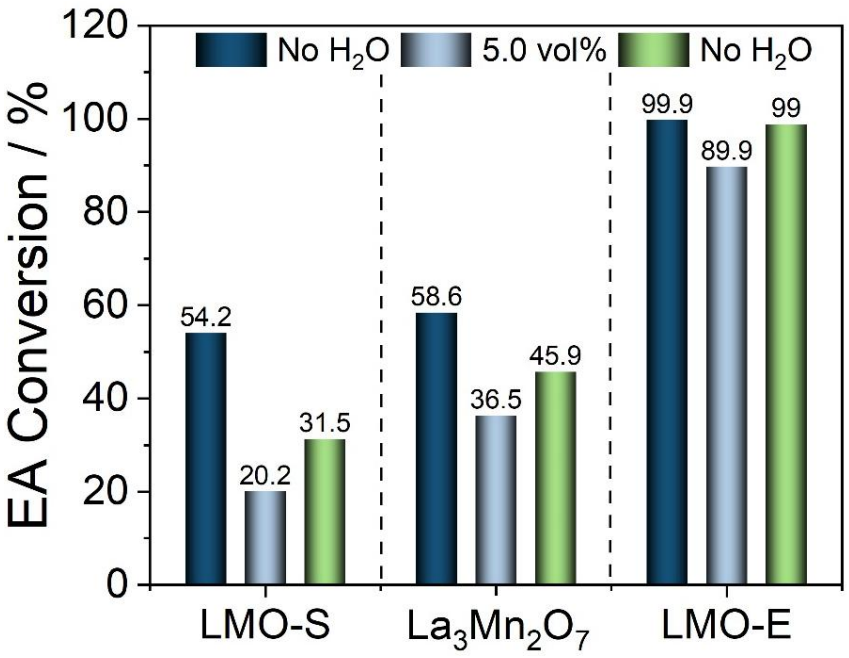


**Supplementary Figure 12.** EA conversions obtained from LMO-S, $La_3Mn_2O_7$ and LMO-E, with and without introducing water vapor.

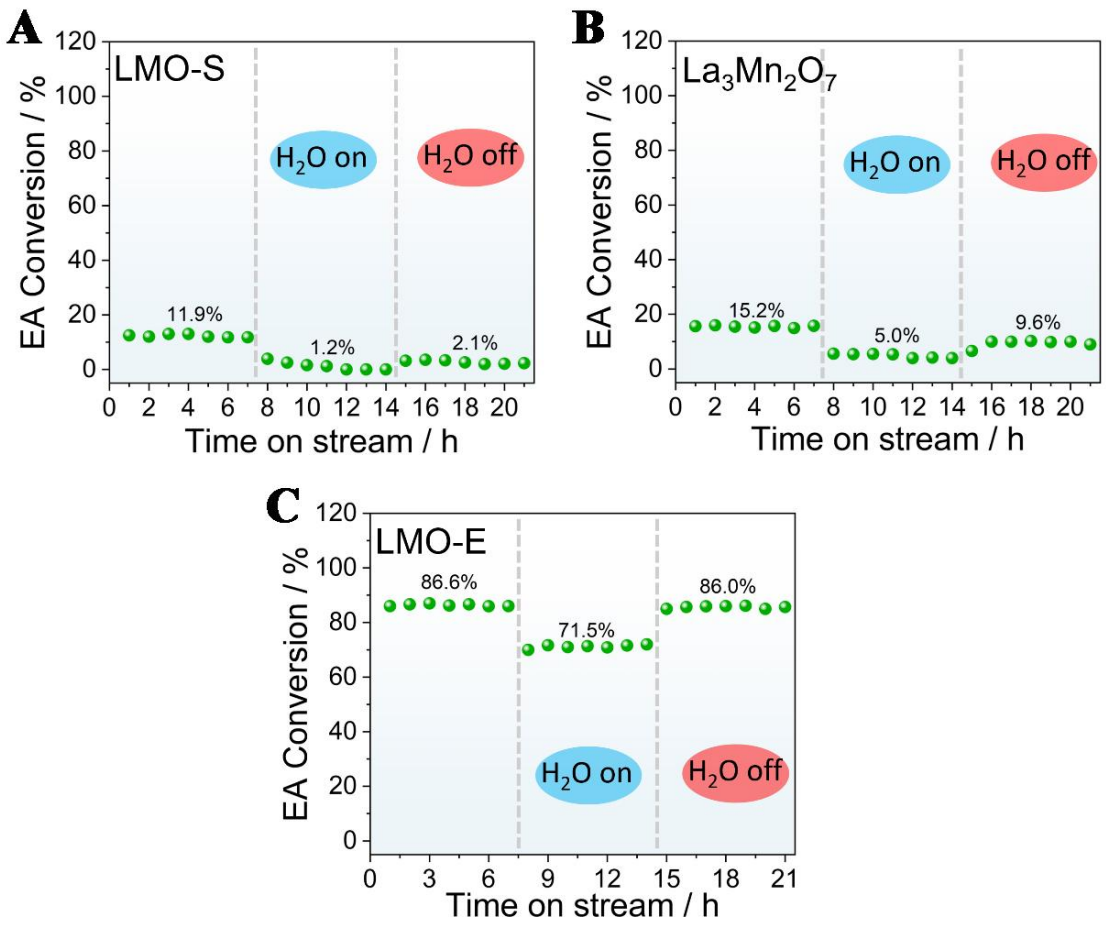


**Supplementary Figure 13.** Effects of 5.0 vol % water vapor on the catalytic activity of (A) LMO-S, (B) $La_3Mn_2O_7$, (C) LMO-E for EA oxidation, conducted at 185 °C.

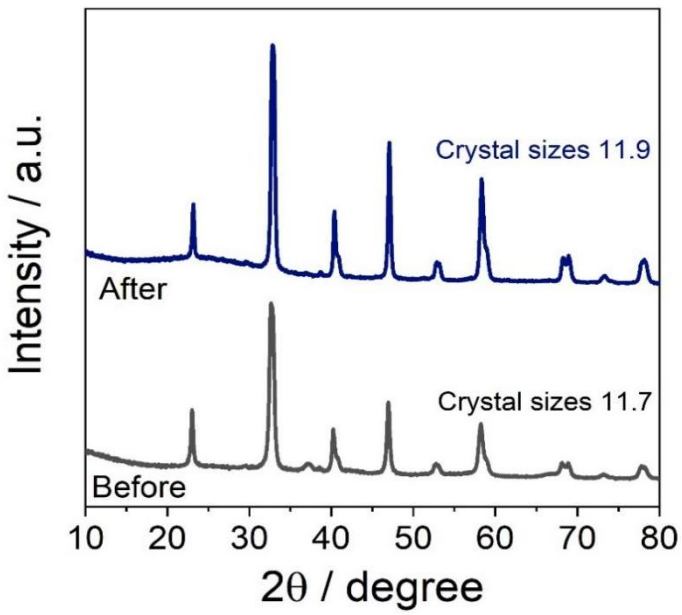


**Supplementary Figure 14.** XRD patterns of LMO-E before and after the long-term stability experiment for EA oxidation at 185 °C.

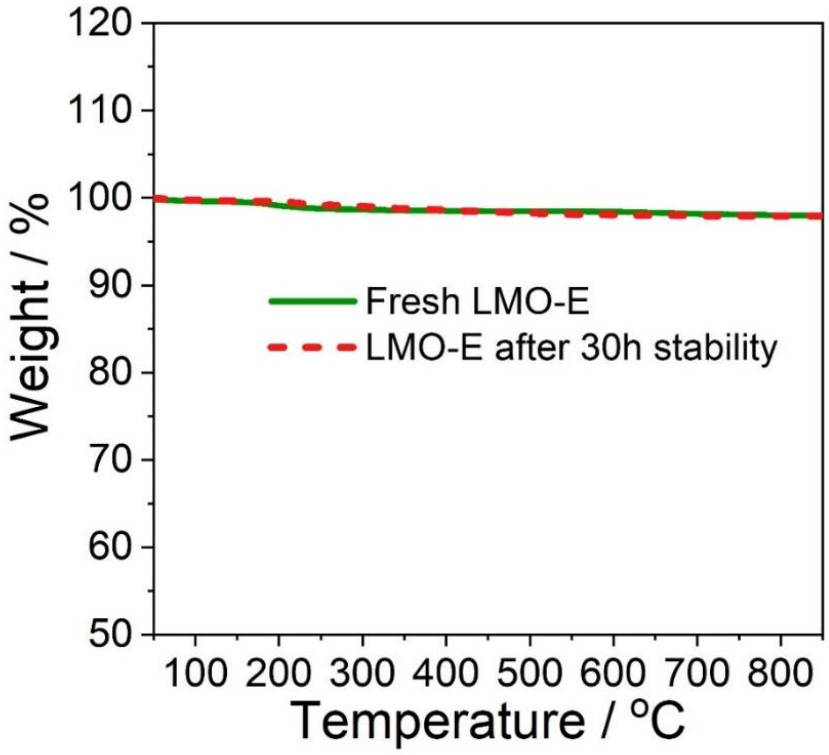


**Supplementary Figure 15.** TGA profiles of LMO-E before and after the long-term stability experiment for EA oxidation at 185 °C.

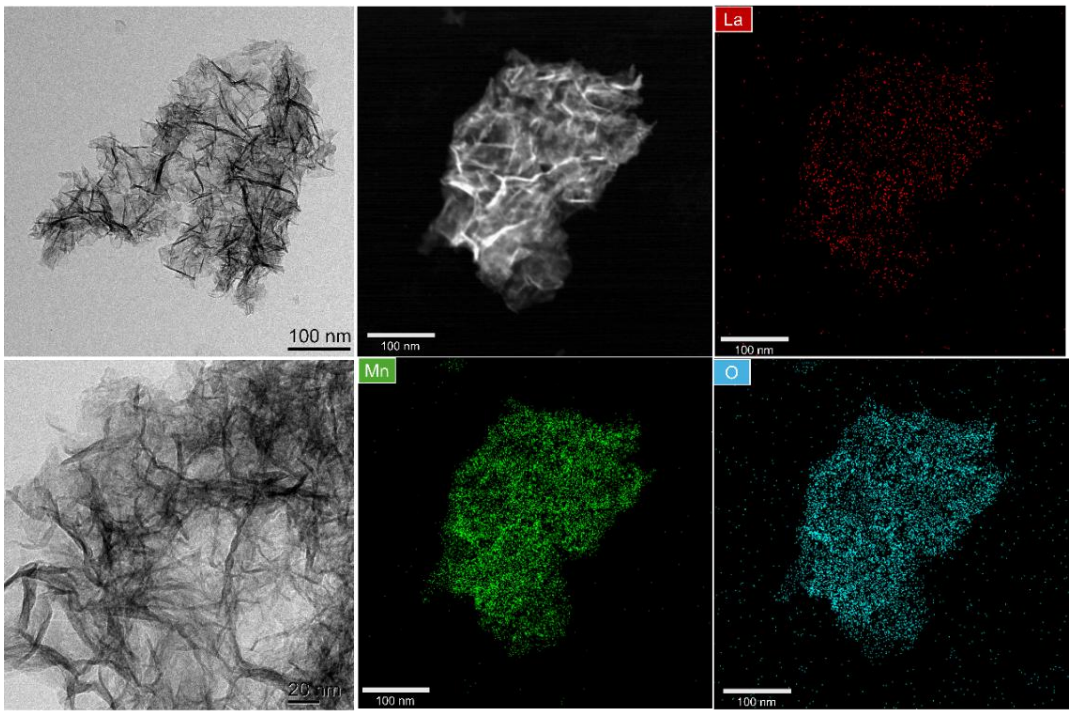


**Supplementary Figure 16.** HRTEM and EDS mapping images of LMO-E after the long-term stability experiment for EA oxidation at 185 °C.

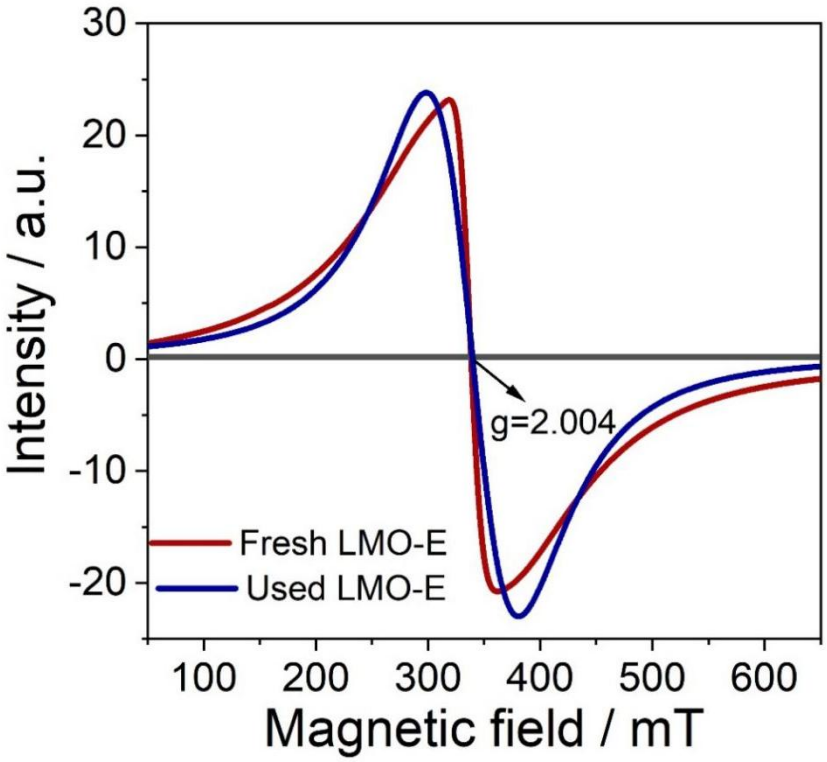


**Supplementary Figure 17.** EPR spectra of LMO-E after the long-term stability experiment for EA oxidation at 185 °C.

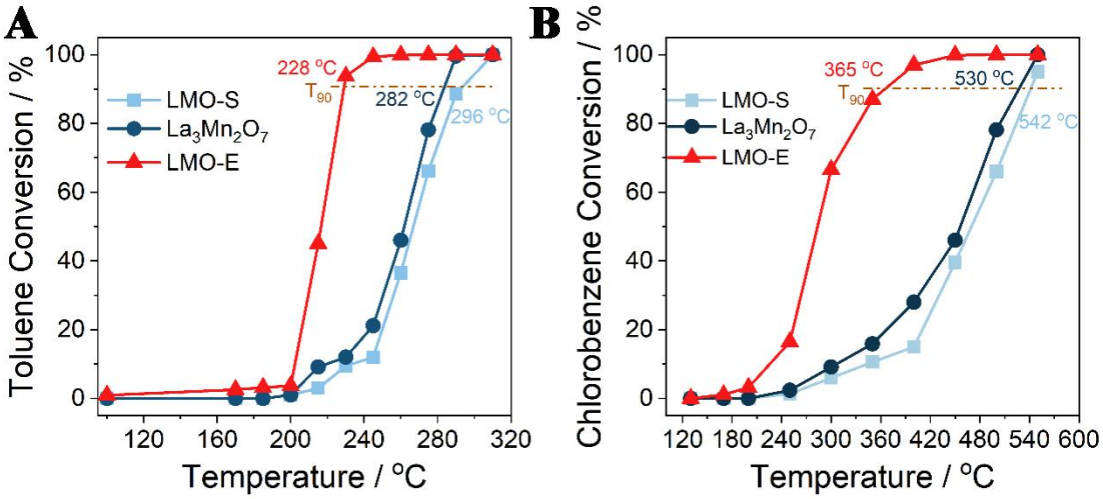


**Supplementary Figure 18.** Conversion of (A) toluene and (B) chlorobenzene obtained from LMO-S, LMO-E and $La_3Mn_2O_7$.

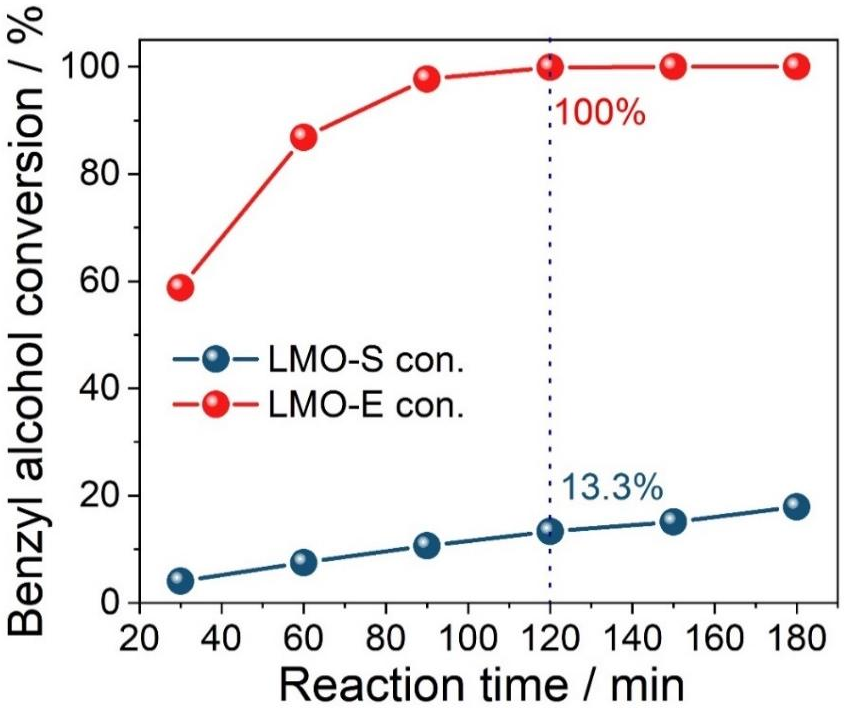


**Supplementary Figure 19.** Catalytic performances of LMO-S and LMO-E for aerobic selective oxidation of benzyl alcohol to benzaldehyde.

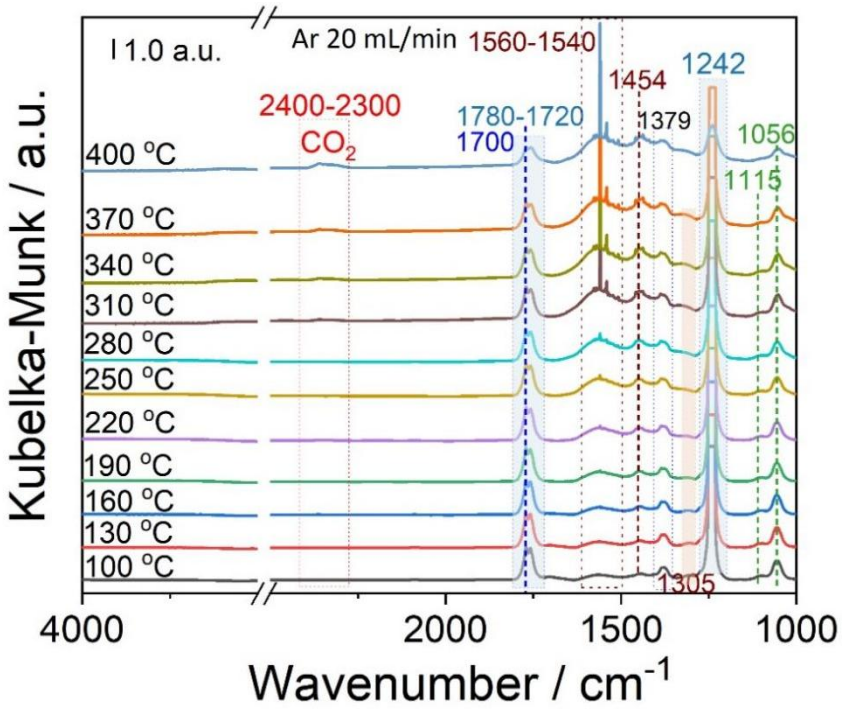


**Supplementary Figure 20.** Temperature-dependent *in situ* DRIFTS profiles of EA oxidation conducted over LMO-E.

**Supplementary Table 1. Textural properties of LMO-E, LMO-S and $La_3Mn_2O_7$**

| Samples | Crystal sizes (nm) | La/Mn ratio | $H_2$ consumption (mmol $g^{-1}$) |
|---|---|---|---|
| LMO-S | 16.1 | 1.01 | 2.43 |
| LMO-E | 11.7 | 0.75 | 9.31 |
| $La_3Mn_2O_7$ | 14.2 | 1.49 | 2.92 |

**Supplementary Table 2. Surface compositions of LMO-E, LMO-S and $La_3Mn_2O_7$, data obtained from XPS spectra**

| Sample | La (%) | Mn (%) | O (%) | Mn $2p_{3/2}$ | O 1s |
|---|---|---|---|---|---|
| | | | | $Mn^{4+}/Mn^{3+}$ | Ov |
| LMO-S | 14.41 | 15.64 | 69.96 | 1.06 | 17.67 |
| $La_3Mn_2O_7$ | 17.29 | 6.73 | 75.97 | 1.13 | 23.93 |
| LMO-E | 6.81 | 20.94 | 72.25 | 1.31 | 36.86 |

**Supplementary Table 3. Fitting results of O1s XPS spectra for LMO-E, LMO-S and $La_3Mn_2O_7$**

| Sample | $O_{adv}$ | $O_{surf}$ | $O_v$ | $O_L$ |
|---|---|---|---|---|
| LMO-S | 2.76 | 13.18 | 17.67 | 66.39 |
| $La_3Mn_2O_7$ | 0.49 | 7.37 | 23.93 | 68.21 |
| LMO-E | 3.21 | 2.33 | 36.86 | 57.6 |

**Supplementary Table 4. EXAFS fitting parameters at the Mn *K*-edge for Mn-foil, $MnO_2$, LMO-E and LMO-S**

| Sample | Shell | *CN*[a] | *R*(Å)[b] | $\sigma^2$(Å$^2$)[c] | $\Delta E_0$(eV)[d] | *R* factor |
|---|---|---|---|---|---|---|
| Mn-foil | Mn-Mn | 4* | 2.406±0.001 | 0.0258 | 0.7 | 0.0084 |
| | Mn-Mn | 3* | 2.628±0.001 | 0.0089 | | |
| $MnO_2$ | Mn-O | 6.0±0.2 | 1.881±0.003 | 0.0025 | 0.5 | 0.0066 |
| | Mn-Mn | 3.3±0.3 | 2.842±0.006 | 0.0053 | -8.8 | |
| | Mn-Mn | 5.9±0.3 | 3.439±0.004 | 0.0024 | 0.1 | |
| LMO-E | Mn-O | 3.2±0.3 | 1.900±0.002 | 0.0041 | -0.8 | 0.0026 |
| | Mn-Mn | 2.2±0.3 | 3.082±0.003 | 0.0115 | 9.4 | |
| | Mn-La | 4.8±0.7 | 3.210±0.006 | 0.0082 | -4.3 | |
| LMO-S | Mn-O | 4.6±0.2 | 1.946±0.004 | 0.0070 | -3.7 | 0.0077 |
| | Mn-Mn | 6.3±0.6 | 3.500±0.008 | 0.0213 | 3.8 | |
| | Mn-La | 2.8±0.2 | 3.680±0.004 | 0.0027 | -1.4 | |

[a]*CN*, coordination number; [b]*R*, the distance to the neighboring atom; [c]$\sigma^2$, the Mean Square Relative Displacement (MSRD); [d]$\Delta E_0$, inner potential correction; *R* factor indicates the goodness of the fit. $S0^2$ was fixed to 0.761, according to the experimental EXAFS fit of Mn foil by fixing *CN* as the known crystallographic value. * This value was fixed during EXAFS fitting, based on the known structure of Fe. Fitting range: $3.0 \le k$ (/Å) $\le 11.0$ and $1.5 \le R$ (Å) $\le 2.8$ (Mn foil); $3.0 \le k$ (/Å) $\le 12.0$ and $1.0 \le R$ (Å) $\le 3.5$ ($MnO_2$); $3.0 \le k$ (/Å) $\le 11.0$ and $1.0 \le R$ (Å) $\le 3.5$ (HLS-259-1-Mn); $3.0 \le k$ (/Å) $\le 10.5$ and $1.0 \le R$ (Å) $\le 4.0$ (HLS-259-2-Mn). A reasonable range of EXAFS fitting parameters: $0.700 < S_0^2 < 1.000$; $CN > 0$; $\sigma^2 > 0$ Å$^2$; $|\Delta E_0| < 15$ eV; *R* factor < 0.02.

**Supplementary Table 5. Comparisons in the activities of LMO-E for EA oxidation with the materials reported in literature**

| Catalysts | EA Concen. (ppm) | GHSV ($h^{-1}$) | $T_{90}$ (°C) | Reference |
|---|---|---|---|---|
| LMO-E | 1000 | 50,000 | 184 | This work |
| 5% Mn−$CeO_2$ NBs | 1000 | 30,000 | 189 | [5] |
| 0.26 Pd/3.2 N-$TiO_2$ | 200 | 20,000 | 212 | [6] |
| 5-MI-500 | 1000 | 60,000 | 192 | [7] |
| $MnO_x$-$CeO_2$-s | 500 | 60,000 | 200 | [8] |
| $Ce_{0.5}Mn_{0.5}$ | 1000 | 30,000 | 200 | [9] |
| $CoCe_{0.75}Zr_{0.25}$-NF | 1000 | 60,000 | 227 | [10] |
| $Pd/Al_2O_3$ | 1000 | 50,000 | 277 | [11] |
| $Co_3O_4$@$MnO_x$ | 1000 | 17,000 | 210 | [12] |

**Supplementary Table 6. Assignment of the IR bands**

| **Bands position ($cm^{-1}$)** | **Position Assignment** | **Characteristic of** | **Reference** |
|---|---|---|---|
| 1242 | *v*(C - O) | ethyl acetate | [13] |
| 1780-1720 | *v*(C = O) | ethyl acetate | [14] |
| 1379 | *v*($CH_3$) | primary alcohols or esters | [15] |
| 1056 | *v*(C - O) | primary alcohols or esters | [16] |
| 1560-1540 | *vas*($COO^-$) | surface alcoholates or acetate | [13] |
| 1454 | *vs*($COO^-$) | surface alcoholates or acetate | [7, 10] |
| 1770 | *v*(C = O) | acetic acid | [17] |
| 1305 | *vas*($COO^-$) | primary alcohols or esters | [6] |
| 1115 | *v*(C - O) | primary alcohols or esters | [5] |

*v:* stretching; *δ:* bending*; s*: symmetric; *as*: asymmetric

**REFERENCES**


[1] S. Wang, X. Xu, J. Zhu, D. Tang, Z. Zhao, *J. Rare Earths* **2019**, *37*, 970-977.

[2] X. Du, G. Zou, Y. Zhang, X. Wang, *J. Mater. Chem. A* **2013**, *1*, 8411-8416.

[3] B. Ravel, M. Newville, *J. synchrotron radiat.* **2005**, *12*, 537-541.

[4] S. I. Zabinsky, J. J. Rehr, A. Ankudinov, R. C. Albers, M. J. Eller, *Phys. Rev. B* **1995**, *52*, 2995-3009.

[5] Z. Shen, E. Gao, X. Meng, J. Xu, Y. Sun, J. Zhu, J. Li, Z. Wu, W. Wang, S. Yao, Q. Dai, *Environ. Sci. Technol.* **2023**, *57*, 3864-3874.

[6] X. Wang, L. Wu, Z. Wang, Y. Feng, Y. Liu, H. Dai, Z. Wang, J. Deng, *Appl. Catal. B* **2023**, *322*, 122075.

[7] Y. Ye, J. Xu, L. Gao, S. Zang, L. Chen, L. Wang, L. Mo, *Chem. Eng. J.* **2023**, *471*, 144667.

[8] Y. Jiang, J. Gao, Q. Zhang, Z. Liu, M. Fu, J. Wu, Y. Hu, D. Ye, *Chem. Eng. J.* **2019**, *371*, 78-87.

[9] Y. J. Lao, X. X. Jiang, J. Huang, Z. Zhang, X. Y. Wang, *Rare Met.* **2021**, *40*, 547-554.

[10] M. Ma, X. Feng, R. Yang, L. Li, Z. Jiang, C. Chen, C. He, *Fuel* **2022**, *317*, 123574.

[11] M. Ma, R. Yang, C. He, Z. Jiang, J. W. Shi, R. Albilali, K. Fayaz, B. Liu, *J. Hazard. Mater.* **2021**, *401*, 123281.

[12] Q. Zhao, Y. Zheng, C. Song, Q. Liu, N. Ji, D. Ma, X. Lu, *Appl. Catal. B* **2020**, *265*, 118552.

[13] M. Ma, R. Yang, Z. Jiang, C. Chen, Q. Liu, R. Albilali, C. He, *Fuel* **2021**, *303*, 121244.

[14] a) Y. Qin, X. Liu, T. Zhu, T. Zhu, *Mater. Chem. Phys.* **2019**, *229*, 32-38; b) N. Sundaraganesan, C. Meganathan, B. Karthikeyan, *Spectrochim. Acta, Part A* **2008**, *70*, 430-438.

[15] X. Liu, Q. Han, W. Shi, C. Zhang, E. Li, T. Zhu, *J. Catal.* **2019**, *369*, 482-492.

[16] X. Zhu, S. Zhang, Y. Yang, C. Zheng, J. Zhou, X. Gao, X. Tu, *Appl. Catal. B* **2017**, *213*, 97-105.

[17] Y. Zheng, Q. Zhao, C. Shan, S. Lu, Y. Su, R. Han, C. Song, N. Ji, D. Ma, Q. Liu, *ACS Appl. Mater. Interfaces* **2020**, *12*, 28139-28147.